

# Perceptual Requirements for World-Locked Rendering in AR and VR

PHILLIP GUAN, Reality Labs Research, Meta, United States of America  
ERIC PENNER, Reality Labs Research, Meta, United States of America  
JOEL HEGLAND, Reality Labs Research, Meta, United States of America  
BENJAMIN LETHAM, Meta, United States of America  
DOUGLAS LANMAN, Reality Labs Research, Meta, United States of America

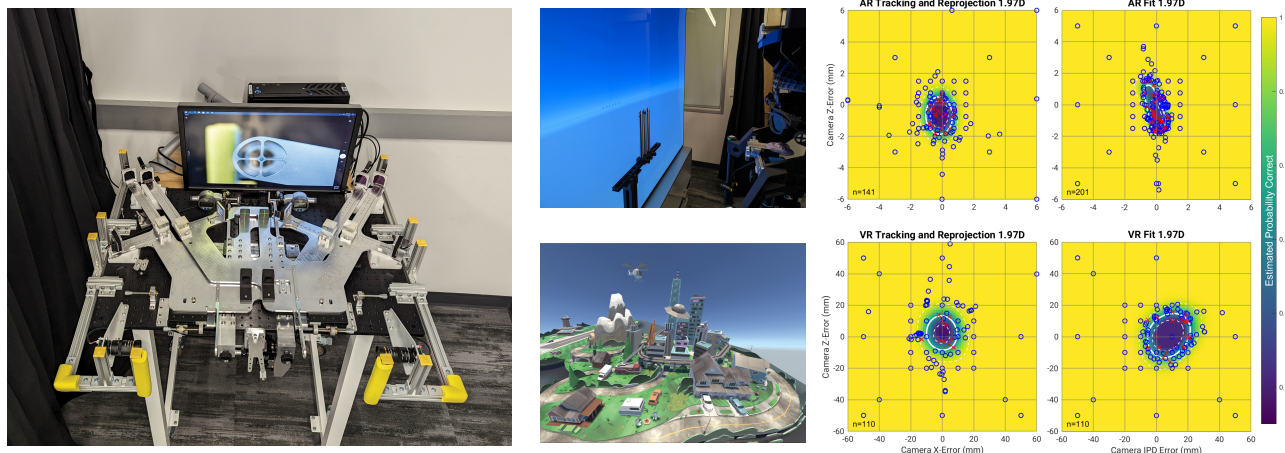


Fig. 1. This work introduces a system with world-locked rendering (WLR) capabilities which is used to run user studies to determine perceptual requirements for WLR in augmented and virtual reality (AR and VR). (Left) A bite bar calibration and measurement system that precisely positions users’ eyes to a known location. This system is used in combination with a recently introduced stereoscopic, wide field of view, distortion-free display to achieve perceptually stable world-locked rendering in AR. (Center Top) The rotating chinrest with bite bar and optical posts used as realworld references in the AR user study. (Center Bottom) The cityscape scene used in the VR user study. (Right) Representative study results showing acceptable headtracking and headset fit errors in AR and VR environments for WLR collected with AEPsych, an adaptive experimentation platform (correct and incorrect trials shown in blue and red respectively).

Stereoscopic, head-tracked display systems can show users realistic, world-locked virtual objects and environments. However, discrepancies between the rendering pipeline and physical viewing conditions can lead to perceived instability in the rendered content resulting in reduced realism, immersion, and, potentially, visually-induced motion sickness. The requirements to achieve perceptually stable world-locked rendering are unknown due to the challenge of constructing a wide field of view, distortion-free display with highly accurate head- and eye-tracking. In this work we introduce new hardware and software built upon recently introduced hardware and present a system capable of rendering virtual objects over real-world references without perceivable drift under such constraints. The platform is used to study acceptable errors in render camera position for world-locked rendering in augmented and virtual reality scenarios, where we find an order of magnitude difference in perceptual sensitivity between them. We conclude by comparing study results with an analytic model which examines changes to apparent depth and visual heading in response to camera displacement errors. We identify visual heading as an important consideration for world-locked rendering alongside depth errors from incorrect disparity.

## 1 INTRODUCTION

One promise of head-mounted displays (HMDs) is the ability to visualize and interact with virtual objects and environments as if they were real. Delivering such immersive experiences with sustained presence requires rendering 3D content with consistent shape, size,

and position. World-locked rendering (WLR) is an important consideration in augmented reality (AR) HMDs because errors in the rendering and presentation pipeline will cause virtual content to move relative to the real world. WLR is also crucial in virtual and mixed reality (VR and MR) headsets because errors in WLR can lead to perceived local or global instability in VR and misregistration of the virtual and real world in MR.

Conceptually, WLR is achieved when stereoscopic images of a virtual environment viewed in an HMD exactly match what an observer would see in an equivalent physical environment from the same viewpoint. If the render cameras used to generate these images are not collocated with the centers of projection (CoP) of the viewer’s left and right eyes when the images are presented, then resulting inconsistencies in perspective geometry between the presented and physically correct binocular images can lead to perceptual errors. In practice, some amount of error will be imperceptible, and in this work we investigate how accurately the render cameras must be positioned and how these requirements vary between AR and VR headsets. Near-eye optics can also introduce additional distortions to rendered images during image presentation. However, the root cause and compensation for such distortions are distinct from the systems affecting accurate render camera placement so they are not

considered in this work, but have been studied by others [Guan et al. 2022; Kuhl et al. 2008; Tong et al. 2019, 2020].

A number of geometric models that attempt to quantify potential errors when render and view locations are not the same have been proposed [Held and Banks 2008; Holloway 1997; Hwang and Peli 2019; Rolland et al. 2004; Wann et al. 1995; Woods et al. 1993]. However, geometric analysis alone cannot elucidate the perceptual consequences of these distortions. For example, the visual system can estimate surface slant from the frames of paintings or bezels of flat-panel displays to partially compensate for distortions from off-axis viewing [Banks et al. 2014; Vishwanath et al. 2005].

A major impediment in defining WLR requirements is that studies cannot be conducted using HMDs because errors in headtracking, eyetracking, and optical distortion correction inherently limit a system’s ability to achieve WLR. Vision science studies, which usually prioritize stimulus fidelity, do not generalize well to WLR because accuracy in these studies is generally achieved by stabilizing the user’s head. Temporally inconsistent view errors during head movements lead to apparent motion, which is more easily detected than static misalignment [Mckee and Nakayama 1984]. Additionally, user head and body movements introduce visual-vestibular cue integration, which influences how inaccurate visual cues are interpreted [Butler et al. 2010; Cuturi and MacNeilage 2014; Fetsch et al. 2009; Fulvio et al. 2021; MacNeilage et al. 2012]. These investigations highlight the importance of studying WLR with active observers (i.e., allowing for some degree of natural eye and head movements), further complicating hardware requirements and experimental design for WLR studies. Thus, one of the most basic requirements underpinning the effectiveness of all augmented and virtual reality headsets remains unresolved. In this work we address these concerns and present the first user study on WLR requirements with active observers using a world-locked-rendering capable system. This is accomplished with the following contributions:

- We introduce a bite bar calibration platform and build upon a recently introduced head and eyetracked, distortion-free, wide field of view stereoscopic display system to render completely world-locked virtual objects over physical references while users rotate their heads and maintain fixation on the physical reference (i.e., a vestibulo-ocular reflex eye movement).
- We design and run a user study using the newly introduced hardware to derive perceptual requirements for world-locked rendering in AR and VR headsets, providing the first direct comparison of such requirements. We further investigate the implications of different errors (e.g., interpupillary distance compared to translation errors) and viewing conditions (viewing distance and virtual environment).
- We compare study results to a geometric model and identify visual direction, rather than disparity or depth errors, as a potential predictor for WLR errors in VR.

## 2 RELATED WORK

*User Studies on Render Camera Placement.* One of the earliest works explicitly evaluating the impacts of incongruent viewing and rendering positions was conducted by Pollock et al. [2012]. They

found incorrect depth and distance percepts in a cave automatic virtual environment (CAVE) when viewing content away from the CoP of the renderer. They note that the perceived errors were smaller than predicted compared to geometric modeling. Ponto et al. [2013] describe a user-in-the-loop calibration for a VR HMD to improve WLR with optimized rendering parameters. With this procedure they report more accurate depth judgments and reduced spatial drift from different viewpoints, but the values obtained for interpupillary distance (IPD) in their user-calibrated method are, on average, 16mm larger than measured values. This suggests that their parameters were compensating for other sources of error.

A recurring discussion in 1990s HMD research was whether parallax from millimeter-scale movement of the user’s CoP during an eye rotation was perceptually significant [Holloway 1997; Rolland et al. 2004; Wann et al. 1995]. These small shifts, coined *ocular parallax* by Brewster [1845] over 100 years earlier, have been a topic of recent interest, and studies have found them to be detectable under certain conditions [Konrad et al. 2020; Krajancich et al. 2020; Lee et al. 2015]. Importantly, all existing work on WLR has been in display systems with optical distortions and/or inaccurate head and eyetracking systems. Furthermore, these studies are also conducted with stationary observers. The hardware, software, and user study described in this work address these two concerns and our results provide additional context for when different types and magnitudes of error are important to consider in AR and VR headsets.

*Perception Research using Headsets.* Perceptual research conducted in HMDs is limited by tracking capabilities in available hardware, so studies have primarily focused on what users perceive while wearing headsets. El Jamiy and Marsh [2019] and Creem-Rhegar et al. [2023] survey many of these recent studies, which are often related to how accurately depth is perceived. Most studies find that depth is underperceived in HMDs, but due to limits in tracking accuracy and distortion correction, it is difficult to determine how much this phenomenon can be attributed to shortcomings in hardware [Itoh et al. 2021] or to geometric errors in incorrect stereoscopic image rendering and presentation. Wilmott et al. [2022] conducted a study on WLR using a commercially available AR HMD (HoloLens 2). They added 10Hz noise to world-locked objects and found that users could detect this motion at 1-3arcmin amplitudes. Although limited by the tracking and rendering systems in the HoloLens 2, these results provide a notable point of comparison for our study results in Section 4.

*Other Cues to Depth.* Underperceived depth is not limited to headsets. Binocular disparity is a relative depth cue, and disparity alone cannot be used to recover metric depth. A significant body of work in vision science has studied what additional visual cues the visual system uses to estimate absolute depth from disparity. Even under well-controlled settings, depth is underperceived without monocular texture cues (i.e., using random dot stereograms and other perspective-free stimuli) [Bradshaw et al. 1996; Cumming et al. 1991; Guan and Banks 2016; Johnston 1991]. With the introduction of perspective cues, Hartle and Wilcox [2022] compared real objects with their rendered counterparts, and with these stimuli, subjects were able to perceive accurate depth in virtual environments-provided

they viewed the real world scenes first. Zhong et al. [2021] go further, and use a multifocal plane display with high dynamic range to create rendered images that are indistinguishable from reality under specific viewing conditions. Their use of the multifocal plane display is important because accommodation and defocus cues have been shown to be as important as disparity in depth perception [Burge and Geisler 2011; Held et al. 2012; Watt et al. 2005; Zannoli et al. 2016]. While our study investigates the importance of accurate pictorial cues for depth perception, it is important to remember that fixed-focus displays alone may not be sufficient to achieve complete depth constancy and WLR.

*Acceptable Video See-Through.* Research in video see-through and video passthrough have found that users can adapt to significant mismatches (55-125mm) between the original camera position and the user’s eyes [Biocca and Rolland 1998; Lee et al. 2013], and even larger errors are possible with perceptual adaptation over the course several days [Lee and Park 2020]. Our work aims to determine the smallest errors leading to inaccurate depth perception and does not consider potential adaptation of the visual system to suprathreshold errors. Adaptation may improve user experience in VR and MR HMDs, but will not resolve WLR conflicts in AR.

### 3 A TESTBED FOR WORLD-LOCKED RENDERING

We introduce a system capable of WLR for active observers to support a comprehensive study of render camera displacement tolerances in AR and VR. This system is designed to track a user’s left and right eye CoP with sufficient precision to achieve WLR; predict where each CoP will be when images are presented and use this position for rendering; and present content stereoscopically on a wide FOV display to emulate HMD-like viewing conditions, without distortion. We take inspiration from the system described by Guan et al. [2022], which addresses the distortion-free, wide FOV display requirement to replicate VR viewing and make several hardware and software additions to their head and eyetracking model for vestibulo-ocular reflex (VOR) in order to achieve WLR.

#### 3.1 Criteria for World-Locked Rendering

Before describing our hardware and software components, we first define the perceptual target and performance criteria for our final system. In AR, real-world objects act as stable, ground-truth references against potential instability of virtual objects, and we exploit this to build an end-to-end validation test of the WLR system. Three optical posts, separated laterally by 2.24cm, are placed 0.64D in front of the display at 1.97D and three 5mm virtual spheres are rendered to float just above a 4mm threaded insert in the center of each posts (top middle column Figure 1). The display and fixation distances are selected to mimic a realistic scenario for hands-based interaction with a varifocal display [Padmanaban et al. 2017], so the posts are intentionally located at the edge of the Zone of Comfort [Shibata et al. 2011]. When accurate rendering parameters are used, the spheres will remain stabilized over the posts when the user moves their head and eyes. Any errors in the system cause the virtual spheres to drift relative to each threaded insert [Azuma and Bishop 1994]. We considered our system capable of WLR when the three virtual

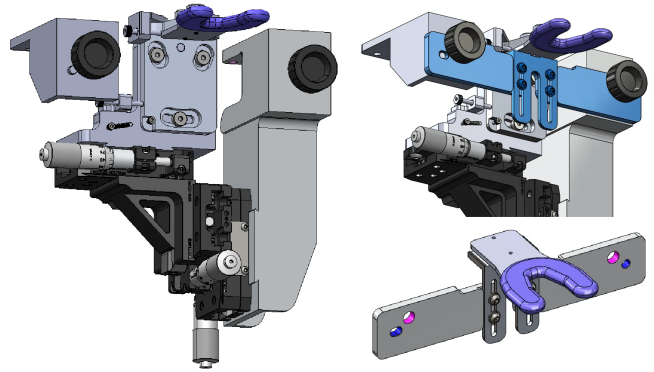


Fig. 2. *Five Degree-of-Freedom Bite Bar Platform.* (Left) Translation and roll adjustments on the adjustment stage. (Right) After the bite bar calibration and measurement are complete, a standard baseplate (in blue) is attached to the bite bar carrier and transferred to the rotating chin rest in the middle column of Figure 1. The baseplate acts as a shared frame of reference across the calibration platform and the rotating chin rest, ensuring that the calibration process is valid across both devices.

spheres appear completely stationary over the posts during a VOR eye movement.

#### 3.2 Bite Bar Calibration Platform

The system described by Guan et al. [2022] measures eye position during a VOR eye movement by combining head rotation with a known gaze point to estimate eye positions. This algorithm is dependent on using an accurate head and eye model for each participant, and in their implementation a bite bar is used to stabilize each user’s head when presenting 3D content off the plane of their display (but not for planar content on the display). We attempted to use their bite bar system and determined that it was not precise enough to facilitate WLR in an augmented reality environment.

We improve the accuracy of this VOR tracking model with new bite bar calibration and measurement hardware seen in Figure 1. This hardware allows each bite bar to position a user’s head within the rotating chin rest (top middle column Figure 1) at the same, nominal eye relief. Our design is inspired by Hillis and Banks [Hillis and Banks 2001] who used a six degree-of-freedom bite bar and subjective user task on a sighting device to position the centers of rotations (CoR) of users’ eyes at the same location. Our bite bar has five degrees of freedom and uses a camera-based alignment system to precisely place each user’s corneal apex to the same, nominal eye relief (see supplementary videos). User bite bars are affixed to a high precision 3D translation stage (Figure 2) and this stage is used to move users’ heads to a target location. This position is achieved by aligning the left and right corneal apices with sighting targets monitored by two high resolution cameras, which can be seen on the monitor in Figure 1. The bite bar holder has additional yaw and roll adjustments. An iterative process between rotational and translation adjustment is used to guide both eyes to the target locations. Once proper alignment is achieved, users align a cross through a bore site for each eye to measure the left and right eye lateral positions, which is cross-referenced with an interpupillary distance (IPD) measurement from a pupilometer. The bite bar is

secured to a baseplate with adhesive (Loctite HY 4070), and the entire module is transferred to the rotating chin rest in Figure 1.

### 3.3 Accurate Latency Prediction

The updated bite bar system improved WLR performance, but it did not completely eliminate apparent drift between the virtual and real objects. We further improved the VOR tracking model by introducing a second-order Savitzky-Golay filter for forward prediction. The predictive filter is necessary to better match the camera positions used for rendering to the user’s CoP during frame presentation compared to the original outlined implementation which relies on the fast 1000Hz update rate of the rotary encoder to reduce latency. Prior to adding the filter, we first optimized our software stack to reduce total latency and characterized it using the NVIDIA Reflex ecosystem, reaching a reported value of 16.67ms which can be accounted for by one frame (8.33ms) of rendering and one frame for image back buffering. The most stable percept of the test scene in Section 3.1 was achieved with 26ms of forward prediction, and the additional 10ms of latency can most likely be attributed to one frame of processing on the OLED panel and 1-2ms of latency from reading the rotary encoder over USB.

### 3.4 End-to-End System Validation

Even with the updated bite bar system and latency optimization and compensation, a discerning observer could note a small amount of drift in the WLR test scene. Krajancich et al. [2020] allowed users to make small, fine-tuned adjustments to align virtual and physical content in their AR study condition. In our case we were able to achieve WLR during VOR once users were allowed to make small (1-2mm) adjustments to align the optical post positions to the virtual spheres during a one-time alignment with their heads in the nominal viewing position at zero degree rotation. To achieve maximum accuracy, an adjustable height chin rest could have been used to firmly affix each viewer’s lower jaw to the bite bar to further minimize head movement. With additional pressure from the chin rest, the virtual spheres had zero apparent drift during VOR head and eye movement. We elected to prioritize user comfort during studies, and did not employ this method; so, in practice, naive observers who were not trained or motivated to stabilize their heads within the rotating chin rest system could experience incomplete WLR. However, each of the 11 participants in our user study reported that the nadir of the 5mm spheres remained above the 4mm threaded posts, indicating WLR to within 2.5mm for each subject. We only screened subjects based on visual and stereo acuity, so we believe subjective WLR could be achieved across the general population in our testbed.

## 4 WORLD-LOCKED RENDERING USER STUDIES

We next describe a psychophysical user study with active observers to determine perceptual sensitivity to render camera position errors on WLR using the introduced testbed. Additional study details and raw data are presented in Section 1 of the supplementary materials.

### 4.1 Stimulus and Task

Detectable render camera displacement was identified using a two-interval forced choice task (2IFC). In one interval render cameras were co-located with the CoP and in the other interval render cameras were displaced from the CoP. Participants were asked to fixate on a specified gaze target during a horizontal VOR eye movement, but they were not instructed to make their VOR movements with any particular magnitude or frequency. They controlled the speed, duration, and magnitude of their head rotation. The virtual scene varied depending on experimental settings, but within each condition, scenes were identical in each interval with the exception of render camera displacement. The two intervals were randomly ordered and subjects were asked to identify which interval appeared more world stable and, for VR scenes, less distorted. When render camera position errors led to artifacts below a detectable threshold, subjects would identify the distorted interval at chance (50%) and at 100% when errors led to easily detectable artifacts. Auditory feedback was provided after each trial to indicate whether participants correctly identified the trial with render camera displacement. Acceptable camera placement was defined by the errors that could be accurately identified 75% of the time.

### 4.2 User Study Modeling and Threshold Extraction

We used AEPsych [Owen et al. 2021] to collect data and learn a model for the user response (probability the error was detected) as a function of lateral and longitudinal camera displacement. For response curve modeling, camera displacement was represented in polar coordinates and the model enforced monotonicity in detection probability with respect to displacement magnitude; see the supplementary materials for more details. Thresholds were computed by inverting the model and finding displacements that produced a 75% detection probability.

### 4.3 Comparison of Augmented and Virtual Reality

In this first experiment render camera placement requirements are derived for AR and VR viewing conditions. The AR scene is described in Section 3.1 and users were instructed to fixate at the top of the threaded screw in the center optical post. During piloting the posts were removed for the VR viewing condition and the same scene was used to measure sensitivity to render camera errors. However, this scene was too sparse, and without full-FOV content to provide relative motion cues, motion in the three spheres was too difficult to detect. The VR scene used instead is shown in Figure 1, and the fixation point is located on a cartoon person at the center of the image. The scene is positioned so that the fixation point is located on the plane of the display.

Render camera displacements are simulated independently in each eye, and the relative displacement of the cameras has distinct perceptual consequences. In the lateral dimension opposite sign errors represent an IPD error and same sign errors are equivalent to a headtracking error to the left or right. In the longitudinal axis same sign errors represent an error in eye relief, and opposite sign errors place the render cameras at different depths, slightly magnifying one eye’s image relative to the other. In the vertical dimension same sign errors represent an error in the user’s height and opposite sign errors

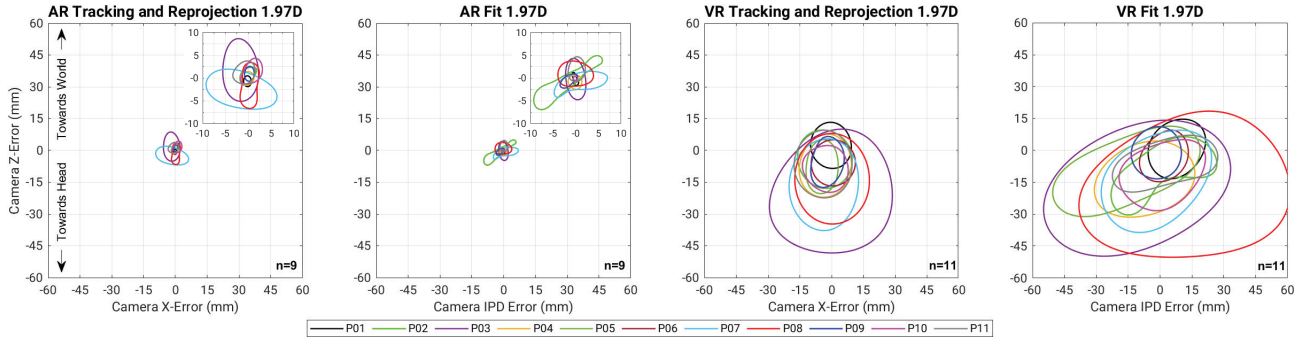


Fig. 3. *Render Camera Displacement Thresholds for Near Display.* Thresholds for camera displacement relative to both eye’s CoP leading to disruptions in WLR for a 1.97D display. In all conditions errors along the ordinate affect the relative longitudinal offset between the user’s eyes and render cameras (i.e., eye relief). Positive values are towards the display and negative values are towards the user. For tracking conditions Camera X-Error represents a leftwards or rightwards shift in camera position in the rotated head’s frame of reference. For fit conditions an IPD error represents the total error in camera baseline relative to the user’s true IPD, also in the rotated head’s frame of reference (e.g., a +10mm IPD error is an outwards shift of each render camera relative to the user’s eyes).

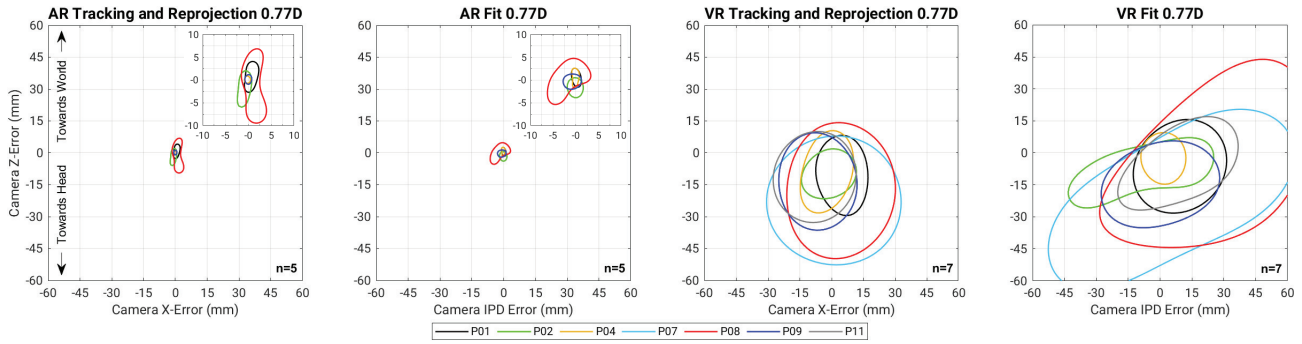


Fig. 4. *Render Camera Displacement Thresholds for Far Display.* Thresholds for camera displacement relative to both eye’s CoP leading to disruptions in WLR for a 0.77D display. Data was collected for the same subjects as the near display condition, but a smaller subset of subjects participated in this study due to time constraints and availability for followup data collection sessions.

introduce a global vertical disparity shift. The testbed hardware does not allow vertical head movement, so errors in the vertical axis are not considered in this study. From these six potential errors, two combinations of interest were selected. The first represents head-tracking or camera reprojection errors that displace the user’s head and are simulated with same sign errors in the lateral and longitudinal axes (x-error and z-error respectively). The second represents headset fit errors which occur when the assumed IPD and eye-relief values used in rendering are not accurate.

User sensitivity to tracking and fit errors are shown for AR and VR conditions in Figure 3. Two subjects, P07 and P08, were not able to reliably identify camera displacements at the  $\pm 15\text{mm}$  displacement limits set in the AEPsych model for the AR condition, so an accurate model could not be fit to their data and their AR results are excluded from the figure. Using the area within each participant’s thresholds to define acceptable camera displacement, AR tolerances for tracking and fit errors are  $31.4\text{mm}^2 \pm 36.5\text{mm}^2$  and  $21.1\text{mm}^2 \pm 18.2\text{mm}^2$ . The same thresholds are more than an order of magnitude larger

in VR,  $7.6\text{cm}^2 \pm 7.0\text{cm}^2$  and  $17.0\text{cm}^2 \pm 15.8\text{cm}^2$ , respectively. Unsurprisingly, a paired t-test across the nine participants who successfully completed both AR and VR conditions shows a statistical difference between the thresholds (AR:  $26.3\text{mm}^2 \pm 28.5\text{mm}^2$ , VR:  $13.4\text{cm}^2 \pm 13.7\text{cm}^2$ ,  $p=.0007$ ). Sensitivity to errors are not statistically significant when comparing tracking and fit conditions in AR ( $p=.35$ ), but are significant in VR ( $p=.02$ ). Considering the ordinate is the same for tracking and fit conditions, this indicates that lateral tracking errors disrupt WLR more than IPD errors; a surprising finding further explored in Section 5.

Another notable asymmetry between the AR and VR conditions is an apparent bias towards negative eyerelief in VR. We compute the centroid of each subject’s acceptable camera displacement errors, and in AR there are no significant biases away from zero error, but in VR eye-relief errors in both tracking and fit conditions are significantly biased away from zero (tracking:  $-8.5\text{cm}^2 \pm 6.2\text{cm}^2$ ,  $p=.001$ ; fit:  $-9.4\text{cm}^2 \pm 6.5\text{cm}^2$   $p=.0007$ ). Taken together, these results indicate that real world references in AR appear to ground render camera positions errors for WLR; errors are centered around zero and thresholds are equivalent between simulated fit and tracking errors. Once physical references are removed in VR, tracking and

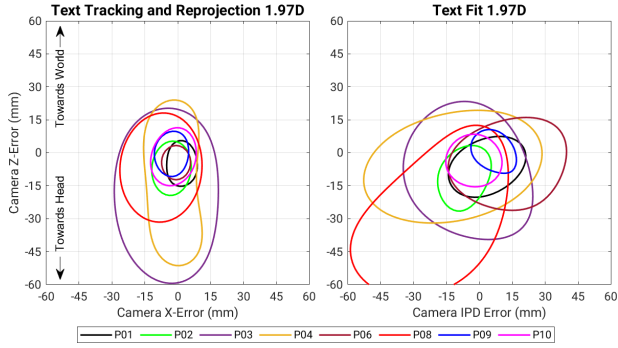


Fig. 5. *Render Camera Displacement Thresholds for Text.* Detectable camera displacement in millimeters relative to user CoP positions at the near display distance, but while viewing a plane of slanted text instead of the city scene in Figure 1.

fit errors are not equivalent, and camera eye-relief errors appear to improve the subjective experience of WLR.

#### 4.4 Virtual Display Distance

The same camera errors will often lead to larger error for a near display distance [Rolland et al. 2004]. The 1.97D viewing distance used in Section 4.3 is much closer than display distances on commercially available HMDs which are in the 0.5D-1.3D range. We repeat the same protocol as before, and move both the physical world-fixed display and simulated head-fixed display to 0.77D to determine the impacts of virtual display distance on WLR requirements in a configuration more applicable to existing devices. For the AR condition the virtual spheres and optical posts are again 0.64D in front of the display. However, the FOV reduction of the display at the farther viewing distance forces a tradeoff between maintaining the same depth range (in diopters) or seeing the entire scene. When the virtual environment is enlarged to maintain depth, a significant portion of the scene is cropped at the larger scale, relative distortions between objects at different depths are no longer visible. We therefore elected to show the same scene without increasing its size (the prominent features in the scene near the fixation point extend approximately  $\pm 30\text{cm}$  away from the display surface at both viewing distances). Five participants repeated the AR conditions and seven repeated the VR conditions due to subject availability and time constraints (Figure 4). The average area for acceptable error at the two viewing distances was compared using a paired t-test yielding no significant difference in sensitivity at the near display distance ( $16.2\text{mm}^2 \pm 6.9\text{mm}^2$ ) and far distance ( $19.2\text{mm}^2 \pm 21.8\text{mm}^2$ ) for AR ( $p=0.61$ ). There was a significant difference for VR at the near distance ( $11.4\text{cm}^2 \pm 12.6\text{cm}^2$ ) compared to the far distance ( $20.5\text{cm}^2 \pm 17.9\text{cm}^2$ ,  $p=0.01$ ). However, it is unclear if the reduced sensitivity can be attributed to the change in display distance or reduction in dioptric scene depth.

#### 4.5 VR Scene Content

Previous work [Guan et al. 2022] found stronger user sensitivity to optical distortions in VR while viewing text compared to a more irregular and less familiar 3D scene. We conduct this comparison

for our final study. Content located at the render display plane is invariant to errors in render camera position [Rolland et al. 2004]; a head-fixed plane of text at the display plane will always be rendered correctly (i.e., always on the display surface), regardless of differences in render and viewing geometry. In our testbed a world-fixed plane is still located at the display plane when a user’s head is not rotated, so render errors will be small when the head rotation is near zero. We rendered a slanted plane of text to compensate for this effect, and the angle is selected to match the slant of the empirical vertical horopter which is  $12.8^\circ$  at 1.97D [Aizenman et al. 2022; Cooper et al. 2011]. We again compare acceptable camera error in the two scenes with a paired t-test find no significant difference (city:  $12.7\text{cm}^2 \pm 14.7\text{cm}^2$ ; text  $13.3\text{cm}^2 \pm 12.5\text{cm}^2$ ,  $p=.79$ ).

## 5 ANALYTIC MODELING

Here we implement an analytic model similar to others identified in Section 2. This model uses binocular perspective projection geometry to identify geometric errors arising from disagreement between render and viewing positions for points within the horizontal meridian defined by the eyes and gaze point. The model works in three stages. First, the viewers head position, orientation, and gaze point are established and the eye model from Krajancich et al. [2020] is used to establish each eye’s CoP location. Render cameras are placed at each CoP and the camera projection plane is set to the simulated virtual display distance. Ground truth disparities and visual direction are then computed for all points in the scene. In the second pass, render cameras are displaced relative to each eye’s CoP and points throughout the horizontal meridian are again projected onto the camera projection planes. These inaccurate 2D projections for the left and right eyes are used to calculate erroneous disparity and heading information when viewed from the true CoP positions. In the final stage, the ground truth disparities and visual directions are compared to these values to compute geometric errors for depth and heading. In this model the origin is represented by the original location of the user’s cyclopean head when their head is un-rotated, and the angular plots shown in Figures 6 and 7 do not account for small changes in the cyclopean eye’s position and rotation during head rotation. The plots also include a 0.6D range around the display plane representing the Zone of Comfort and, in the disparity plot, Panum’s Area is shown representing an approximate region where the visual system can fuse binocular images. Conditions for fusion vary across a number of parameters so this model is primarily meant for illustrative purposes. The criteria for fusion was 20arcmin at the fovea [Palmer 1961] with a linear increase to 60arcmin at six degrees [Hampton and Kertesz 1983; Mitchell 1966; Palmer 1961]. After six degrees fusion limits increase by 7% per degree of eccentricity [Crone and Leuridan 1973; Mitchell 1966].

*Disparity and Visual Direction.* WLR in AR requires accurate alignment in depth and visual direction, and this is reflected in Section 4.3 with results demonstrating equal sensitivity to errors in IPD and lateral displacements in AR. The same results show that these lateral tracking errors are more perceivable than IPD errors when there is not a real-world reference. The columns in Figure 6 show errors in world space and both disparity and heading errors in angular and dioptric space when render and view geometries are mismatched.

The top row shows a simulation for -12mm camera IPD error and the bottom row simulates a -12mm translation error. The most apparent and obvious distortion is in the world view reconstruction in the top left panel, when camera and user IPDs are mismatched. However, our user study results indicate that the errors in the bottom simulation are more perceivable than the top simulation, and it seems that errors in visual direction are more problematic for WLR than depth from disparity errors. Additional insight into this unexpected result can be found in supplemental videos of the same simulations over the course of a  $\pm 20^\circ$  VOR head and eye movement. In these videos the depth distortions from IPD error cause significant shifts in the reconstructed blue squares compared to the intended gray squares defined by the render geometry. However, because the simulated IPD error is symmetric in both eyes, the visual direction of the blue squares is relatively unaffected. Conversely, the blue squares drift from side to side when simulating tracking error and visual sensitivity to this motion could explain why tracking errors are more detectable than IPD errors. One potential explanation for this phenomenon is that depth cues from motion parallax, which are relatively unaffected by IPD errors, help counteract the inaccurate depth cues from binocular disparity when there is IPD error.

*Comparison to Existing Hardware.* Next we consider how thresholds from Section 4 compare to capabilities of existing HMDs. Tracking performance and fit statistics are not readily available, so we instead turn to previous research. The most analogous study to ours was conducted by Wilmott et al. [2022] who added 10Hz sinusoidal motion in a random direction to world-locked objects in HoloLens 2. They found that this motion was detectable at 1-3arcmin amplitude for seated observers viewing a  $10^\circ$  floating cube. This protocol is not directly comparable to ours, as their observers were stationary and were tasked to detect when world-locked cubes appeared to move. The continuous 10Hz motion added to the cubes is likely more detectable than the errors we simulated. However, the tracking and display systems of the HoloLens 2 also make errors in WLR more difficult to detect (potential tracking error, limited display resolution, waveguide color non-uniformity). Nonetheless, this was the most relevant measure of WLR in an existing device that we could find. Our data show -1.5mm of error in camera relief and IPD error are detectable for about half our observers in AR. We examine the impacts of these errors in the geometric model (Figure 7) and see that such errors induce a 4arcmin disparity error at the fixation point and total change in visual direction of 3.6arcmin. Similarly, -1.5mm eye relief and -1.5mm tracking errors lead to 3.3arcmin of visual direction change and disparity errors ranging from 0 to 0.9arcmin at the fixation point. The magnitude of these errors are well above thresholds for stereo and visual acuity, but our AR conditions also included 0.64D of vergence-accommodation conflict. While our results are similar to Wilmott et al. [2022], further investigation is necessary to more directly compare their 10Hz positional jitter stimulus to our stimulus with rendering errors tied to head and eye position.

## 6 DISCUSSION AND FUTURE WORK

We present a world-locked-rendering-capable system achieved with the introduction of a novel bite bar fabrication and calibration hardware. Using this WLR testbed, we ran the first user study protocol to directly compare the perceptual requirements for render camera placement in WLR for AR and VR viewing environments. The study results are analyzed in the context of a perspective-projection based model and we identify apparent visual direction as an important, and previously overlooked, consideration for WLR in VR. We conclude with closing thoughts on our study and potential implications for future HMD design.

*Hardware Limitations.* The OLED display used in the testbed achieves a wide FOV without distortions introduced by near-eye optics. However, the use of the display results in practical limitations for our simulator, including: crosstalk in the 3D shutter glasses; temporal artifacts from time-multiplexed stereoscopic image presentation at 120Hz; and changes in focal distance and resolution as the head moves. The accuracy of our head and eyetracking model relies heavily on the head stabilization achieved with the bite bar. User compliance on the bite bar is not guaranteed, and even when the bite bar is used properly, head movement is still possible. Our results show sensitivity to camera errors in the millimeter range and the stabilization provided by the bite bar system is likely similar, especially for observers who have not used a bite bar before. Head stabilization with the bite bar can be improved, but mostly at the expense of comfort, and discomfort can also affect data quality in multi-hour experiments.

*Further Investigations into VR IPD Errors.* Two follow-up studies to investigate the relationship between IPD errors and WLR in VR would be of particular interest. One would be to combine the head-tracking and fit conditions into a single three-dimensional search space for AEPsych to investigate the interaction between tracking, IPD, and eye-relief errors. The contribution of depth perception from motion parallax could also be examined further by repeating the AR and VR headtracking conditions monocularly.

*Thin Headsets for Direct Reprojection in Mixed Reality.* Video reprojection in mixed reality compensates for the offset between a user’s eyes and the position of the world-facing cameras. Reprojection algorithms impose additional compute costs and also introduce potential latency and in-filling errors from disocclusion [Chaurasia et al. 2020; Xiao et al. 2022]. A potential alternative which does not suffer from these issues is direct video passthrough without reprojection. This alternative is more feasible with thin headset form factors that can reduce the offset between the user’s eye and passthrough camera. In our study each user was sensitive to camera displacements in eye relief greater than 15mm away from the head (Figures 3 and 4). Thin diffractive optics can minimize VR headset thickness [Maimone and Wang 2020], but even this architecture is unlikely to achieve 15mm total thickness. With this in mind, direct video passthrough most likely cannot achieve complete WLR, but based on prior work in Section 2, might be an acceptable experience.

*Eyetracking in AR and VR HMDs.* In AR tolerances to tracking errors on the order of 1-5mm cause detectable errors in WLR, and it

is necessary to account for ocular parallax to achieve WLR in AR. The same tolerances in VR are 10mm or larger, so compensating for these eye movements are not necessary for WLR in VR. However, optical distortions in VR HMDs can induce geometric artifacts larger than errors from incorrect render camera position [Geng et al. 2018; Robinett and Rolland 1992; Rolland and Hopkins 1993] and eye-tracked dynamic distortion correction (ETDDC) is needed to fully compensate for most VR near-eye optics. Eyetracking requirements for ETDDC are also on the millimeter scale [Guan et al. 2022], so millimeter level accuracy is most likely required in both AR and VR headsets to achieve perceptually stable virtual content, albeit for different reasons.

## ACKNOWLEDGMENTS

Thanks to Carla Romero for assistance in data collection and Michael Shvartsman, Craig Sanders, and Stryker Buffington for assistance with AEPsych.

## REFERENCES

- Avi M. Aizenman, George A. Koulieris, Agostino Gibaldi, Vibhor Sehgal, Dennis M. Levi, and Martin S. Banks. 2022. The Statistics of Eye Movements and Binocular Disparities during VR Gaming: Implications for Headset Design. *ACM Trans. Graph.* (jul 2022). <https://doi.org/10.1145/3549529>
- Ronald Azuma and Gary Bishop. 1994. Improving static and dynamic registration in an optical see-through HMD. In *Proceedings of the 21st annual conference on Computer graphics and interactive techniques*. 197–204.
- Martin Banks, Emily Cooper, and Elise Piazza. 2014. Camera Focal Length and the Perception of Pictures. *Ecological psychology: a publication of the International Society for Ecological Psychology* 26 (05 2014), 30–46. <https://doi.org/10.1080/10407413.2014.877284>
- Frank A Biocca and Jannick P Rolland. 1998. Virtual eyes can rearrange your body: Adaptation to visual displacement in see-through, head-mounted displays. *Presence* 7, 3 (1998), 262–277. <https://doi.org/10.1162/105474698565703>
- Mark F. Bradshaw, Andrew Glennerster, and Brian J. Rogers. 1996. The effect of display size on disparity scaling from differential perspective and vergence cues. *Vision Research* 36, 9 (1996), 1255–1264. [https://doi.org/10.1016/0042-6989\(95\)00190-5](https://doi.org/10.1016/0042-6989(95)00190-5)
- David Brewster. 1845. 1. On the Law of Visible Position in Single and Binocular Vision, and on the representation of Solid Figures by the Union of dissimilar Plane Pictures on the Retina. *Proceedings of the Royal Society of Edinburgh* 1 (1845), 405–406.
- Johannes Burge and Wilson S Geisler. 2011. Optimal defocus estimation in individual natural images. *Proceedings of the National Academy of Sciences* 108, 40 (2011), 16849–16854.
- John S. Butler, Stuart T. Smith, Jennifer L. Campos, and Heinrich H. Bühlhoff. 2010. Bayesian integration of visual and vestibular signals for heading. *Journal of Vision* 10, 11 (09 2010), 23–23. <https://doi.org/10.1167/10.11.23>
- Gaurav Chaurasia, Arthur Nieuwoudt, Alexandru-Eugen Ichim, Richard Szeliski, and Alexander Sorkine-Hornung. 2020. Passthrough+ real-time stereoscopic view synthesis for mobile mixed reality. *Proceedings of the ACM on Computer Graphics and Interactive Techniques* 3, 1 (2020), 1–17.
- Emily A. Cooper, Johannes Burge, and Martin S. Banks. 2011. The vertical horopter is not adaptable, but it may be adaptive. *Journal of Vision* 11, 3 (03 2011), 20–20. <https://doi.org/10.1167/11.3.20>
- Sarah H Creem-Regehr, Jeanine K Stefanucci, and Bobby Bodenheimer. 2023. Perceiving distance in virtual reality: theoretical insights from contemporary technologies. *Philosophical Transactions of the Royal Society B* 378, 1869 (2023), 20210456.
- RA Crone and OMA Leuridan. 1973. Tolerance for aniseikonia. *Albrecht von Graefes Archiv für klinische und experimentelle Ophthalmologie* 188, 1 (1973), 1–16.
- Bruce G. Cumming, Elizabeth B. Johnston, and Andrew J. Parker. 1991. Vertical disparities and perception of three-dimensional shape. *Nature* 349, 6308 (January 1991), 411–413. <https://doi.org/10.1038/349411a0>
- Luigi F. Cuturi and Paul R. MacNeilage. 2014. Optic Flow Induces Nonvisual Self-Motion Aftereffects. *Current Biology* 24, 23 (2014), 2817–2821. <https://doi.org/10.1016/j.cub.2014.10.015>
- Fatima El Jamiy and Ronald Marsh. 2019. Survey on depth perception in head mounted displays: distance estimation in virtual reality, augmented reality, and mixed reality. *IET Image Processing* 13, 5 (2019), 707–712.
- Christopher R. Fetsch, Amanda H. Turner, Gregory C. DeAngelis, and Dora E. Angelaki. 2009. Dynamic Reweighting of Visual and Vestibular Cues during Self-Motion Perception. *Journal of Neuroscience* 29, 49 (2009), 15601–15612. <https://doi.org/10.1523/JNEUROSCI.2574-09.2009>
- Jacqueline M Fulvio, Huiyuan Miao, and Bas Rokkers. 2021. Head jitter enhances three-dimensional motion perception. *Journal of vision* 21, 3 (2021), 12–12.
- Ying Geng, Jacques Gollier, Brian Wheelwright, Fenglin Peng, Yusuf Sulai, Brant Lewis, Ning Chan, Wai Sze Tiffany Lam, Alexander Fix, Douglas Lanman, Yijing Fu, Alexander Sohn, Brett Bryars, Nelson Cardenas, Youngshik Yoon, and Scott McEl-downey. 2018. Viewing optics for immersive near-eye displays: pupil swim/size and weight/stray light. In *Digital Optics for Immersive Displays*, Vol. 10676. International Society for Optics and Photonics, SPIE, 19–35. <https://doi.org/10.1117/12.2307671>
- Phillip Guan and Martin S. Banks. 2016. Stereoscopic depth constancy. *Philosophical transactions of the Royal Society of London. Series B, Biological sciences* 371, 1697 (2016), 20150253–20150253. <https://doi.org/10.1098/rstb.2015.0253>
- Phillip Guan, Olivier Mercier, Michael Shvartsman, and Douglas Lanman. 2022. Perceptual Requirements for Eye-Tracked Distortion Correction in VR. In *ACM SIGGRAPH 2022 Conference Proceedings* (Vancouver, BC, Canada) (SIGGRAPH '22). Association for Computing Machinery, New York, NY, USA, Article 51, 8 pages. <https://doi.org/10.1145/3528233.3530699>
- David R Hampton and Andrew E Kertesz. 1983. The extent of Panum's area and the human cortical magnification factor. *Perception* 12, 2 (1983), 161–165.
- Brittney Hartle and Laurie M. Wilcox. 2022. Stereoscopic depth constancy for physical objects and their virtual counterparts. *Journal of Vision* 22, 4 (03 2022), 9–9. <https://doi.org/10.1167/jov.22.4.9>
- Robert T. Held and Martin S. Banks. 2008. Misperceptions in Stereoscopic Displays: A Vision Science Perspective. In *Proceedings of the 5th Symposium on Applied Perception in Graphics and Visualization*. Association for Computing Machinery, New York, NY, USA, 23–32. <https://doi.org/10.1145/1394281.1394285>
- Robert T. Held, Emily A. Cooper, and Martin S. Banks. 2012. Blur and Disparity Are Complementary Cues to Depth. *Current Biology* 22 (2012), 426–431.
- James M. Hillis and Martin S. Banks. 2001. Are corresponding points fixed? *Vision Research* 41, 19 (2001), 2457–2473. [https://doi.org/10.1016/S0042-6989\(01\)00137-7](https://doi.org/10.1016/S0042-6989(01)00137-7)
- Richard L. Holloway. 1997. Registration error analysis for augmented reality. *Presence: Teleoperators & Virtual Environments* 6, 4 (1997), 413–432.
- Alex D. Hwang and Eli Peli. 2019. Stereoscopic Three-dimensional Optic Flow Distortions Caused by Mismatches Between Image Acquisition and Display Parameters. *Journal of Imaging Science and Technology* 63, 6 (2019), 60412–1–60412–7(7). <https://doi.org/10.2352/j.imagingsci.technol.2019.63.6.060412>
- Yuta Itoh, Tobias Langlotz, Jonathan Sutton, and Alexander Plopsi. 2021. Towards indistinguishable augmented reality: A survey on optical see-through head-mounted displays. *ACM Computing Surveys (CSUR)* 54, 6 (2021), 1–36.
- Elizabeth B. Johnston. 1991. Systematic distortions of shape from stereopsis. *Vision Research* 31, 7 (1991), 1351–1360. [https://doi.org/10.1016/0042-6989\(91\)90056-B](https://doi.org/10.1016/0042-6989(91)90056-B)
- Robert Konrad, Anastasios Angelopoulos, and Gordon Wetzstein. 2020. Gaze-Contingent Ocular Parallax Rendering for Virtual Reality. *ACM Trans. Graph.* 39, 2, Article 10, 12 pages. <https://doi.org/10.1145/3361330>
- Brooke Krajancich, Petr Kellnhofer, and Gordon Wetzstein. 2020. Optimizing Depth Perception in Virtual and Augmented Reality through Gaze-Contingent Stereo Rendering. *ACM Trans. Graph.* 39, 6, Article 269 (Nov. 2020), 10 pages. <https://doi.org/10.1145/3414685.3417820>
- Scott A. Kuhl, William B. Thompson, and Sarah H. Creem-Regehr. 2008. HMD Calibration and Its Effects on Distance Judgments. In *Proceedings of the 5th Symposium on Applied Perception in Graphics and Visualization* (Los Angeles, California) (APGV '08). Association for Computing Machinery, New York, NY, USA, 15–22. <https://doi.org/10.1145/1394281.1394284>
- Joong Ho Lee, Sei-young Kim, Hae Cheol Yoon, Bo Kyung Huh, and Ji-Hyung Park. 2013. A Preliminary Investigation of Human Adaptations for Various Virtual Eyes in Video See-through HMDS. In *Proceedings of the SIGCHI Conference on Human Factors in Computing Systems* (Paris, France) (CHI '13). Association for Computing Machinery, New York, NY, USA, 309–312. <https://doi.org/10.1145/2470654.2470698>
- Joong Ho Lee and Ji-Hyung Park. 2020. Visuomotor adaptation to excessive visual displacement in video see-through HMDS. *Virtual Reality* 24, 2 (2020), 211–221.
- Sangyoon Lee, Xinda Hu, and Hong Hua. 2015. Effects of optical combiner and IPD change for convergence on near-field depth perception in an optical see-through HMD. *IEEE transactions on visualization and computer graphics* 22, 5 (2015), 1540–1554.
- Paul R. MacNeilage, Zhou Zhang, Gregory C. DeAngelis, and Dora E. Angelaki. 2012. Vestibular Facilitation of Optic Flow Parsing. *PLOS ONE* 7, 7 (07 2012), 1–8. <https://doi.org/10.1371/journal.pone.0040264>
- Andrew Maimone and Junren Wang. 2020. Holographic Optics for Thin and Lightweight Virtual Reality. *ACM Trans. Graph.* 39, 4, Article 67 (aug 2020), 14 pages. <https://doi.org/10.1145/3386569.3392416>
- Suzanne P. Mckee and Ken Nakayama. 1984. The detection of motion in the peripheral visual field. *Vision Research* 24, 1 (1984), 25–32. [https://doi.org/10.1016/0042-6989\(84\)90140-8](https://doi.org/10.1016/0042-6989(84)90140-8)
- DE Mitchell. 1966. A review of the concept of “Panum’s fusional areas”. *Optometry and Vision Science* 43, 6 (1966), 387–401.

- Lucy Owen, Jonathan Browder, Benjamin Letham, Gideon Stocek, Chase Tymms, and Michael Shvartsman. 2021. Adaptive Nonparametric Psychophysics. arXiv:2104.09549 [stat.ME]
- Nitish Padmanaban, Robert Konrad, Tal Stramer, Emily A Cooper, and Gordon Wetzstein. 2017. Optimizing virtual reality for all users through gaze-contingent and adaptive focus displays. *Proceedings of the National Academy of Sciences* 114, 9 (2017), 2183–2188.
- DA Palmer. 1961. Measurement of the horizontal extent of Panum’s area by a method of constant stimuli. *Optica Acta: International Journal of Optics* 8, 2 (1961), 151–159.
- Brice Pollock, Melissa Burton, Jonathan W. Kelly, Stephen Gilbert, and Eliot Winer. 2012. The Right View from the Wrong Location: Depth Perception in Stereoscopic Multi-User Virtual Environments. *IEEE Transactions on Visualization and Computer Graphics* 18, 4 (2012), 581–588. <https://doi.org/10.1109/TVCG.2012.58>
- Kevin Ponto, Michael Gleicher, Robert G Radwin, and Hyun Joon Shin. 2013. Perceptual calibration for immersive display environments. *IEEE transactions on visualization and computer graphics* 19, 4 (2013), 691–700.
- Warren Robinett and Jannick P Rolland. 1992. A computational model for the stereoscopic optics of a head-mounted display. *Presence: Teleoperators & Virtual Environments* 1, 1 (1992), 45–62.
- Jannick Rolland, Yonggang Ha, and Cali Fidopiastis. 2004. Albertian errors in head-mounted displays: I. Choice of eye-point location for a near- or far-field task visualization. *J. Opt. Soc. Am. A* 21, 6 (Jun 2004), 901–912. <https://doi.org/10.1364/JOSAA.21.000901>
- Jannick P. Rolland and Terry Hopkins. 1993. *A Method of Computational Correction for Optical Distortion in Head-Mounted Displays*. Technical Report TR93-045. University of North Carolina at Chapel Hill. <http://www.cs.unc.edu/techreports/93-045.pdf>
- Takashi Shibata, Joohwan Kim, David M Hoffman, and Martin S Banks. 2011. The zone of comfort: Predicting visual discomfort with stereo displays. *Journal of vision* 11, 8 (2011), 11–11.
- Jonathan Tong, Robert S. Allison, and Laurie M. Wilcox. 2019. The Impact of Radial Distortions in VR Headsets on Perceived Surface Slant. *Electronic Imaging, Human Vision and Electronic Imaging* 11 (2019), 60409–1–60409–11. <https://doi.org/10.2352/J.ImagingSci.Technol.2019.63.6.060409>
- Jonathan Tong, Robert S. Allison, and Laurie M. Wilcox. 2020. Optical distortions in VR bias the perceived slant of moving surfaces. In *2020 IEEE International Symposium on Mixed and Augmented Reality (ISMAR)*, 73–79. <https://doi.org/doi:10/gkmt46S>
- Dhanraj Vishwanath, Ahna Girshick, and Martin Banks. 2005. Why Pictures Look Right When Viewed from the Wrong Place. *Nature neuroscience* 8 (11 2005), 1401–10. <https://doi.org/10.1038/nn1553>
- John P. Wann, Simon Rushton, and Mark Mon-Williams. 1995. Natural problems for stereoscopic depth perception in virtual environments. *Vision Research* 35, 19 (1995), 2731–2736. [https://doi.org/10.1016/0042-6989\(95\)00018-U](https://doi.org/10.1016/0042-6989(95)00018-U)
- Simon J. Watt, Kurt Akeley, Marc O. Ernst, and Martin S. Banks. 2005. Focus cues affect perceived depth. *Journal of Vision* 5, 10 (12 2005), 7–7. <https://doi.org/10.1167/5.10.7>
- James P. Wilmott, Ian M. Erkelens, T. Scott Murdison, and Kevin W. Rio. 2022. Perceptibility of Jitter in Augmented Reality Head-Mounted Displays. In *2022 IEEE International Symposium on Mixed and Augmented Reality (ISMAR)*, 470–478. <https://doi.org/10.1109/ISMAR55827.2022.00063>
- Andrew J. Woods, Tom Docherty, and Rolf Koch. 1993. Image distortions in stereoscopic video systems. In *Stereoscopic Displays and Applications IV*, Vol. 1915. International Society for Optics and Photonics, SPIE, 36–48. <https://doi.org/10.1117/12.157041>
- Lei Xiao, Salah Nouri, Joel Hegland, Alberto Garcia Garcia, and Douglas Lanman. 2022. NeuralPassthrough: Learned Real-Time View Synthesis for VR. In *ACM SIGGRAPH 2022 Conference Proceedings*, 1–9.
- Marina Zannoli, Gordon D Love, Rahul Narain, and Martin S Banks. 2016. Blur and the perception of depth at occlusions. *Journal of Vision* 16, 6 (2016), 17–17.
- Fangcheng Zhong, Akshay Jindal, Ali Özgür Yöntem, Param Hanji, Simon J. Watt, and Rafal K. Mantiuk. 2021. Reproducing Reality with a High-Dynamic-Range Multi-Focal Stereo Display. *ACM Trans. Graph.* 40, 6, Article 241 (dec 2021), 14 pages. <https://doi.org/10.1145/3478513.3480513>

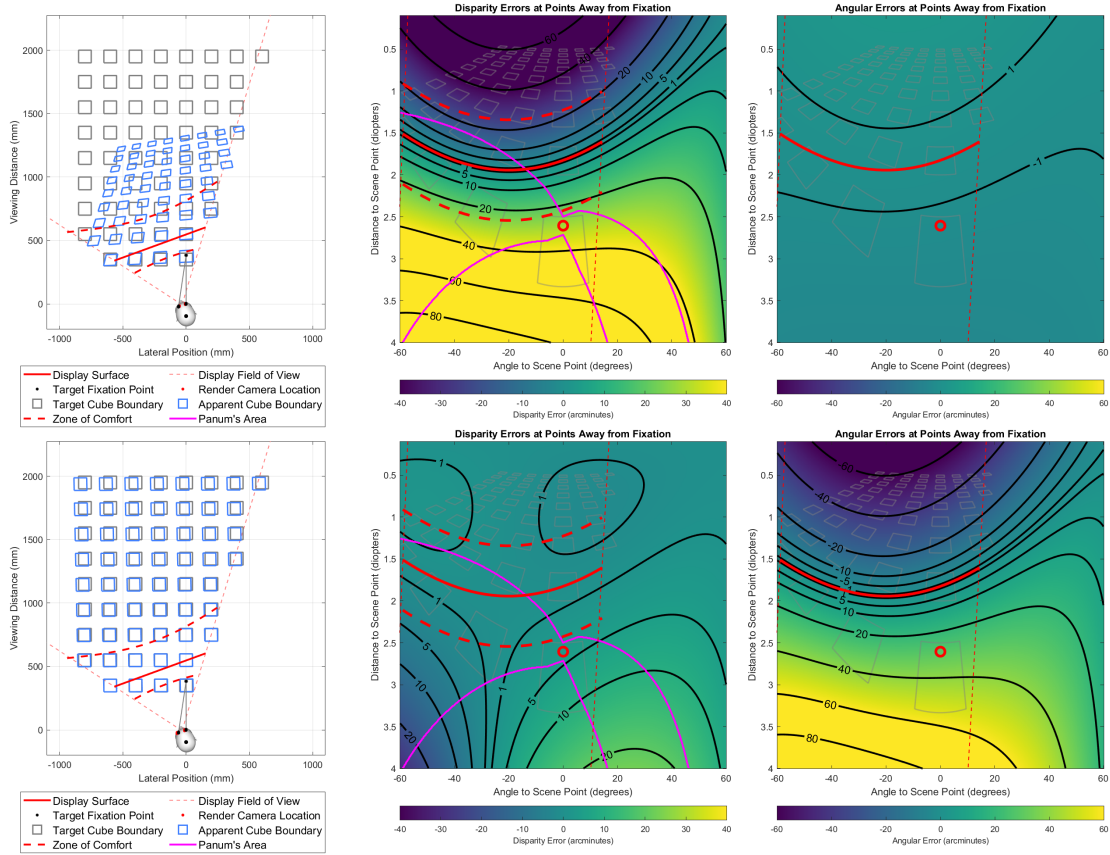


Fig. 6. *Analytic Model of IPD and Tracking Errors in VR.* (Top) A 63mm IPD observer with a  $-20^\circ$  head rotation viewing a scene rendered with 51mm IPD camera baseline. (Bottom) The same user viewing content rendered with a  $-12$ mm displacement instead. (Left) A reconstruction of the scene in world space showing depth and misalignment errors in the scene. (Center) Disparity errors for points away from fixation compared to ground truth. (Right) Errors in visual direction. Our user study shows that the impacts of disparity errors are less apparent to observers compared to changes in visual direction over the duration of a  $\pm 20^\circ$  VOR head movement.

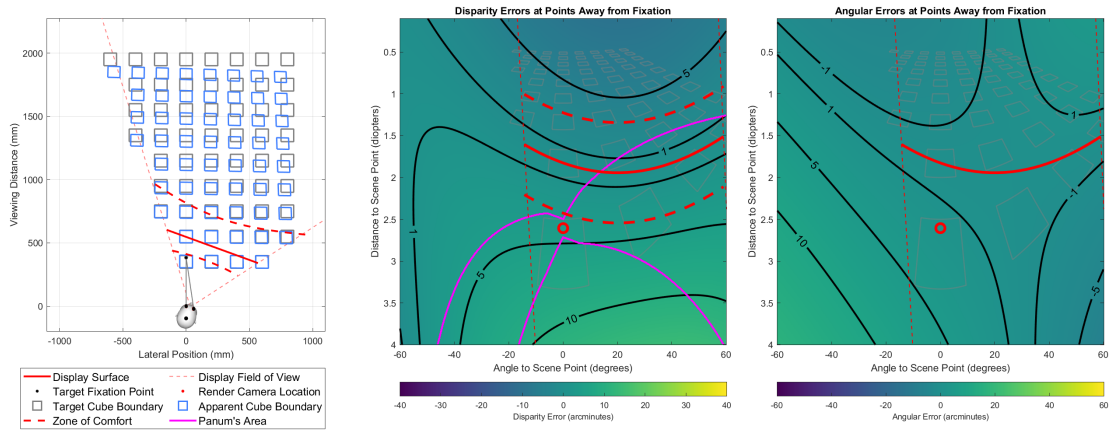


Fig. 7. *Analytic Model of Errors in AR.* The geometric consequences of a 63mm IPD observer with a  $20^\circ$  head rotation viewing a scene rendered with  $-1.5$ mm error in eye relief and  $-1.5$ mm error in camera separation. (Left) A reconstruction of the scene in world space showing depth and misalignment errors in the scene. (Center) Disparity errors for points away from fixation compared to ground truth. (Right) Errors in visual direction. Modeling results show similar thresholds found by Wilmott et al. [2022] using a HoloLens 2. We find similar thresholds in the 1-3arcmin range when applying render camera errors from our results, however, our study protocol and hardware are not directly comparable and similarities in thresholds could be coincidental.

# Perceptual Requirements for World-Locked Rendering in AR and VR

## Supplementary Material

PHILLIP GUAN, Reality Labs Research, Meta, United States of America

ERIC PENNER, Reality Labs Research, Meta, United States of America

JOEL HEGLAND, Reality Labs Research, Meta, United States of America

BENJAMIN LETHAM, Meta, United States of America

DOUGLAS LANMAN, Reality Labs Research, Meta, United States of America

## 1 ADDITIONAL USER STUDY DETAILS

### 1.1 Response Surface Modeling

We used models to estimate the response surface in the user study, probability of detection as a function of camera displacement. As in other recent work [Gardner et al. 2015; Guan et al. 2022; Owen et al. 2021], we used a Gaussian process (GP) as a non-parametric model to flexibly estimate the response surface without specifying a particular form *a priori*. We represent camera displacement in polar coordinates as  $(r, \theta)$ , and denote the probability-of-correct-response function as  $p(r, \theta)$ . We model  $p(r, \theta) = \Phi(f(r, \theta))$  where  $\Phi$  is the Gaussian cumulative distribution function and  $f(r, \theta)$  is a latent response function that has a GP prior. Given data  $\mathcal{D}$  collected in the user study, the GP prior on  $f$  induces a normal posterior distribution  $f(r, \theta) | \mathcal{D} \sim \mathcal{N}(\mu, \sigma^2)$ , whose mean and variance can be computed in closed form.

For the WLR user study, we know that detection probability will be monotonic in the magnitude of the displacement,  $r$ , since larger errors will always be easier to detect. We incorporate that knowledge into the model by enforcing monotonicity in  $f$  with respect to  $r$ . We do so by projecting the posterior distribution in an adaptation of the GP projection method of [Lin and Dunson 2014]. Our method differs from that of [Lin and Dunson 2014] by doing projection of quantiles rather than projection at the sample level, to improve computational efficiency. Specifically, when computing the posterior at  $f(r, \theta)$ , we construct a uniform sequence of  $m + 1$  points  $\tilde{r}_i = \frac{r_i}{m}$ ,  $i = 0, \dots, m$ , that range from 0 up to  $r$ ; we used  $m = 20$  in practice. Denote the posterior at this sequence as  $f(\tilde{r}_i, \theta) | \mathcal{D} \sim \mathcal{N}(\mu_i, \sigma_i^2)$ . We apply a monotonic projection first to the mean at  $(r, \theta)$  by computing  $\hat{\mu} = \max_{i=0, \dots, m} \mu_i$ . We similarly project a lower and upper quantile as  $l = \max_{i=0, \dots, m} \mu_i - 2\sigma_i$  and  $u = \max_{i=0, \dots, m} \mu_i + 2\sigma_i$  respectively. This construction ensures that  $\hat{\mu}$ ,  $l$ , and  $u$  will all be monotonic with respect to  $r$ , for any fixed  $\theta$ . Finally, we use these projected moments as the posterior for  $f(r, \theta)$ : specifically,  $f(r, \theta) \sim \mathcal{N}\left(\hat{\mu}, \left(\frac{u-l}{4}\right)^2\right)$ . If  $f$  was already monotonic with respect to  $r$  then this projection will have no effect, and so with sufficient data the projected posterior distribution will converge to the true, monotonic posterior.

### 1.2 User Study Protocol

We elected to employ a two-interval forced choice (2IFC) protocol shown in Figure 1 to identify the thresholds in our study instead of a faster, but more subjective yes/no task to reduce variability across subjects. Data was collected in two hours per session with subjects coming in for two to four sessions depending on availability. Each condition was run with AEPsych using a 25 to 32 initialization points after which adaptive sampling was used to collect data up to 110 trials. Subjects

collected data in two hour blocks on separate days, and subjects participated in two to five sessions depending on availability. In general subjects were able to complete between three to six different conditions in each two hour block of time. In general we aimed to collect at least 110 trials for each condition, but collected additional trials when time permitted. For adaptive sampling with AEPsych the search limits were set to  $\pm 15\text{mm}$  in AR conditions and  $\pm 60\text{cm}$  for IPD and  $\pm 100\text{mm}$  for eye relief in the VR conditions. For the AR conditions a different maximum value was used to model the data using the method describe in Section 1.1 based on the each subject's sensitivity. This is because using the maximum limits for every subject during model fitting is inefficient for subjects with data clustered near smaller values (e.g the modeled area for P01 in Figure 2, especially for the near display distance, is mostly empty beyond 3mm). The limits used for each participant are represented by the limits shown in the individual raw data plots In Figures 2 through 12.

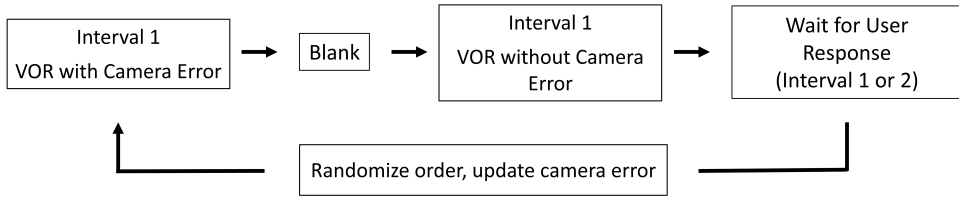


Fig. 1. *Two-interval forced choice procedure*: In the 2IFC task participants compare pupil swim during VOR to a distortion-free reference in every trial compared to a yes/no procedure where subjects compare potential distortion during VOR to a mental model of a distortion-free reference. 2IFC reduces variance across subjects because every trial is compared against the same reference, but increase data collection time.

### 1.3 AR User Study Data

1.3.1 *AR Tracking and Reprojection; Fit; and Viewing Distance*. Here we show data for each participant for all AR conditions.

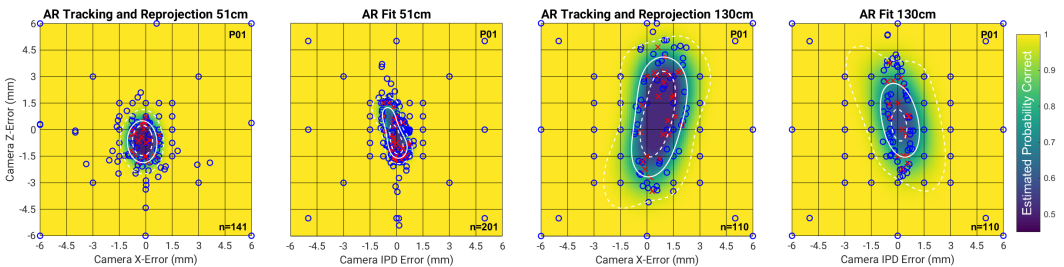


Fig. 2. P01 Raw data for near and far display distances for AR conditions.

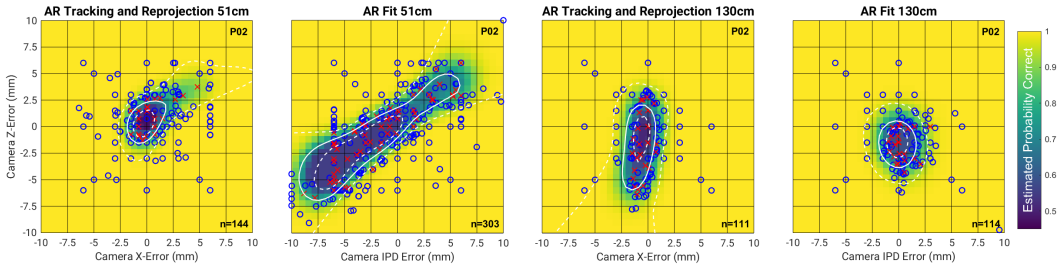


Fig. 3. P02 Raw data for near and far display distances for AR conditions.

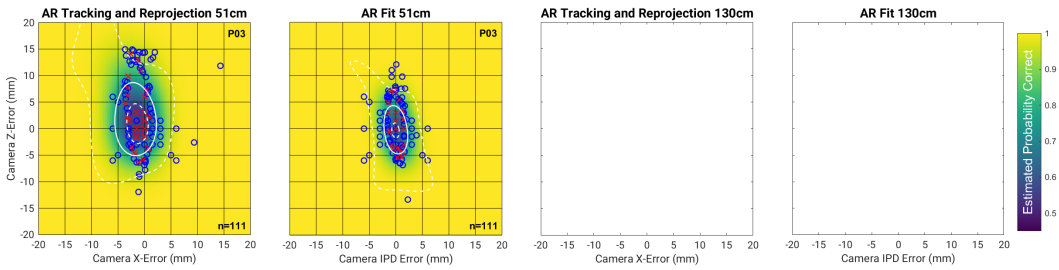


Fig. 4. P03 Raw data for near and far display distances for AR conditions.

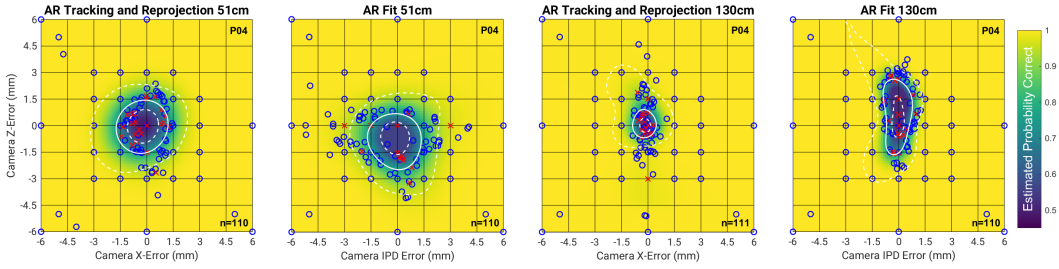


Fig. 5. P04 Raw data for near and far display distances for AR conditions.

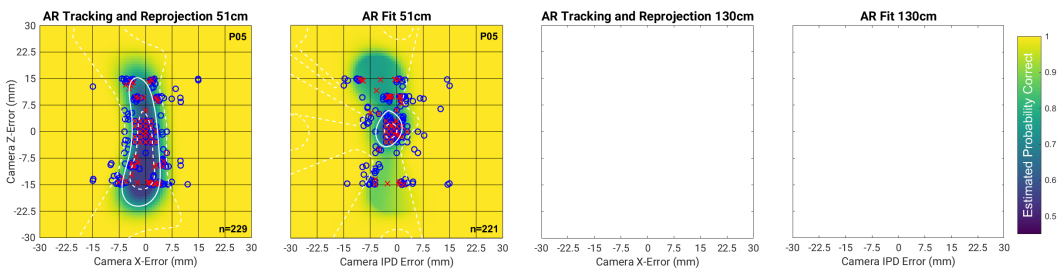


Fig. 6. P05 Raw data for near and far display distances for AR conditions. This subject was not able to reliably complete the AR task at the limits supplied to AEPsych (thresholds are not surrounded by blue circles indicating consistently correct responses) so their AR thresholds are excluded from Figure 3 in the main paper.

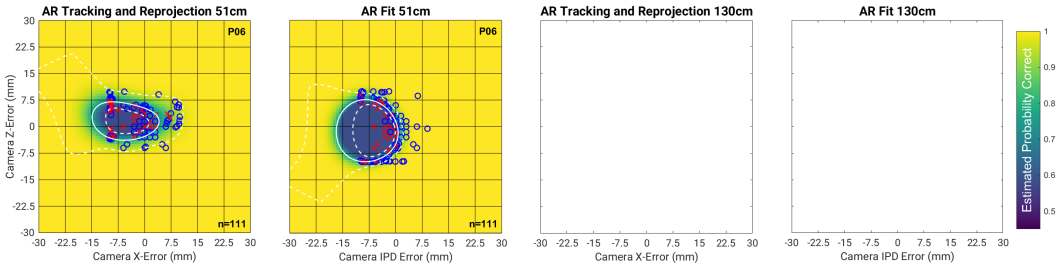


Fig. 7. P06 Raw data for near and far display distances for AR conditions. This subject was not able to reliably complete the AR task at the limits supplied to AEPsych (thresholds are not surrounded by blue circles indicating consistently correct responses) so their AR thresholds are excluded from Figure 3 in the main paper.

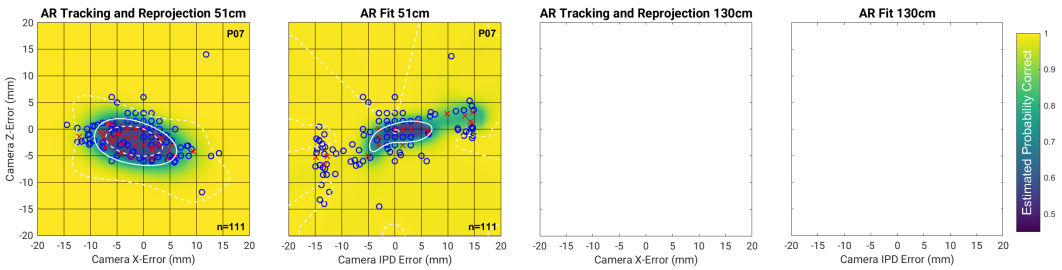


Fig. 8. P07 Raw data for near and far display distances for AR conditions.

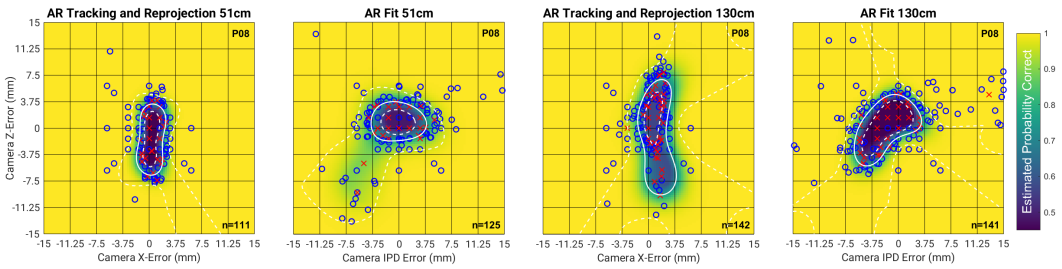


Fig. 9. P08 Raw data for near and far display distances for AR conditions.

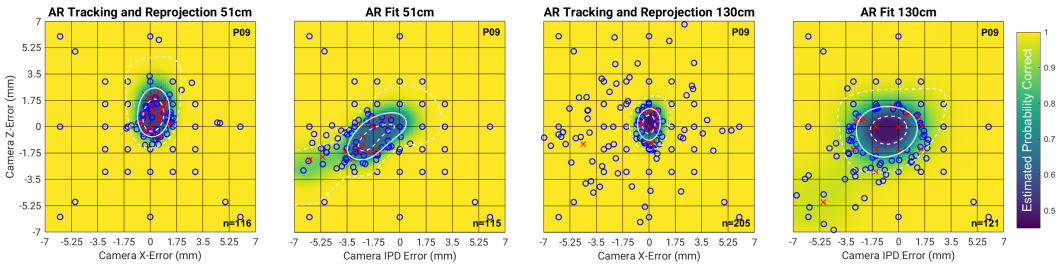


Fig. 10. P09 Raw data for near and far display distances for AR conditions.

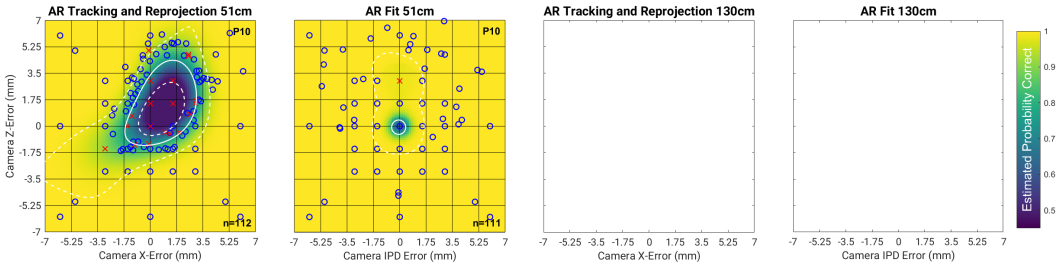


Fig. 11. P10 Raw data for near and far display distances for AR conditions. Note: a lapse trial by this participant and an unusually accurate performance near zero resulted in too many suprathreshold trials for this participant in the AR fit condition. See Section 1.3.2 for more details.

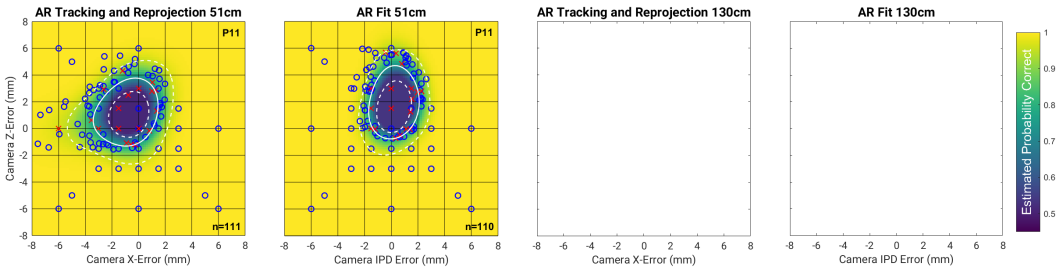


Fig. 12. P11 Raw data for near and far display distances for AR conditions.

**1.3.2 Adaptive Sampling.** Figure 13 shows the trials run for P10. In this instance a lapse trial at a very large value, combined with only a single missed trial near (0,0) resulted in the model sampling large values rather than zero. During data collection we elected to use the built-in Gaussian Process classification model from AEPsych and this model does not have strong priors which means that inefficient sampling can occur in edge cases such as this where a lapse trial and very few missed trials result in the model sampling away from the subject’s true threshold. We did not want to enforce too many priors during data collection and we attempted to prevent such scenarios from occurring by sampling in a fixed grid near (0,0) for initialization trials. However, sensitivity to render camera displacement varied significantly across users, and P10 was more sensitive than other users and in this case the participant only missed a single fixed grid condition. If they had missed a few more trials then the adaptive sampling algorithm would likely have focused on points closer to (0,0).

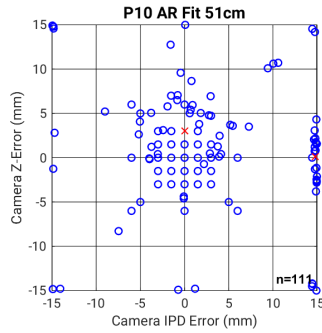


Fig. 13. P10 Lapse trial resulting in poor adaptive sampling.

### 1.4 VR User Study Data

Here we show data for each participant for all VR conditions. In this case we use the same model limit of 80mm for each participant.

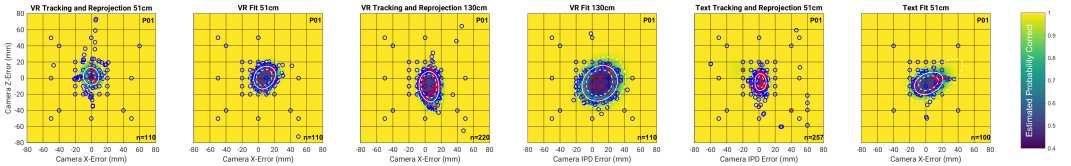


Fig. 14. P01 Raw data for near and far display distances for VR conditions.

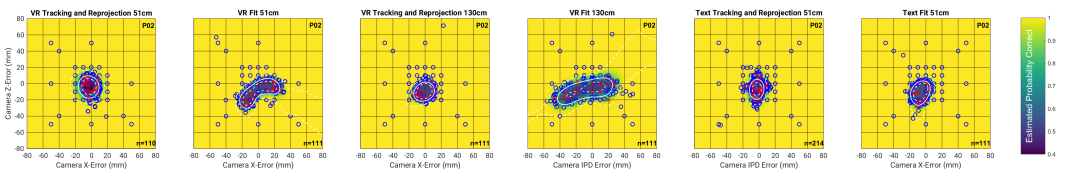


Fig. 15. P02 Raw data for near and far display distances for VR conditions.

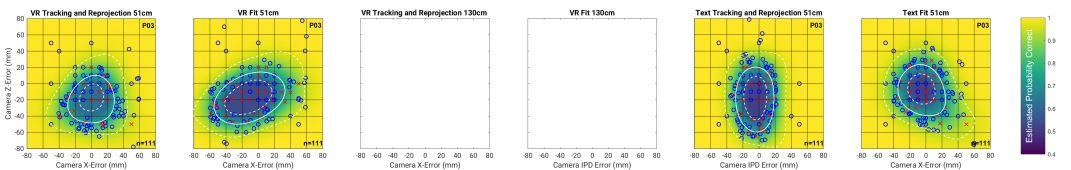


Fig. 16. P03 Raw data for near and far display distances for VR conditions.

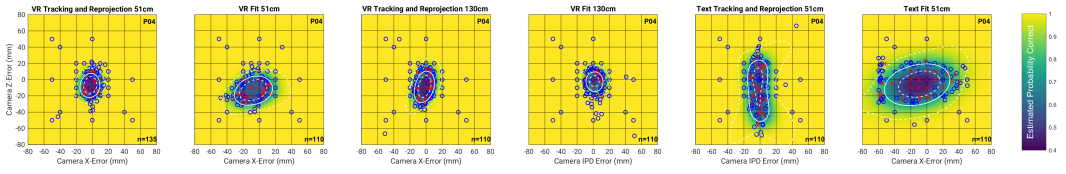


Fig. 17. P04 Raw data for near and far display distances for VR conditions.

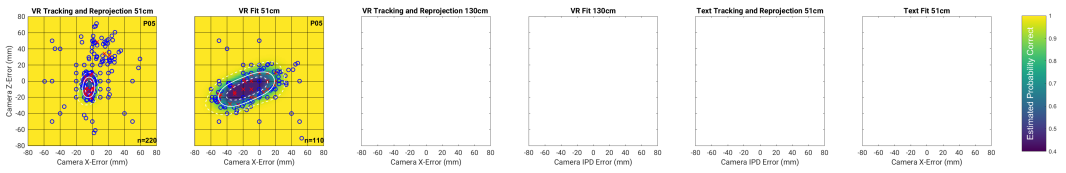


Fig. 18. P05 Raw data for near and far display distances for VR conditions

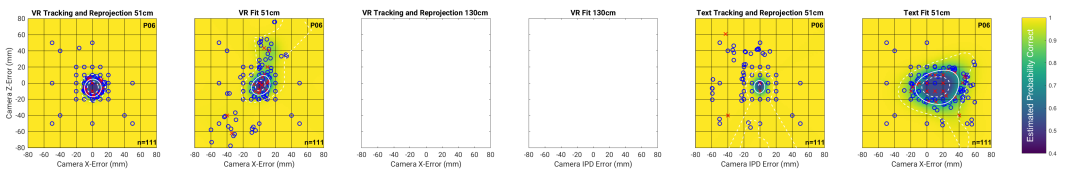


Fig. 19. P06 Raw data for near and far display distances for VR conditions.

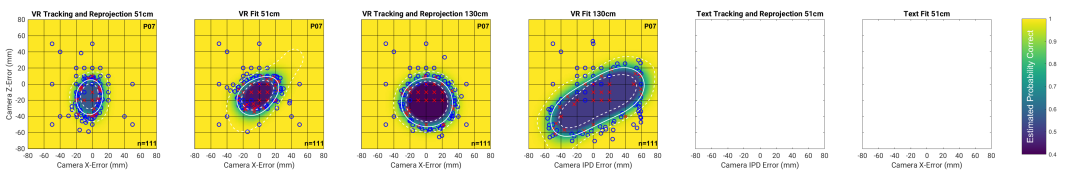


Fig. 20. P07 Raw data for near and far display distances for VR conditions.

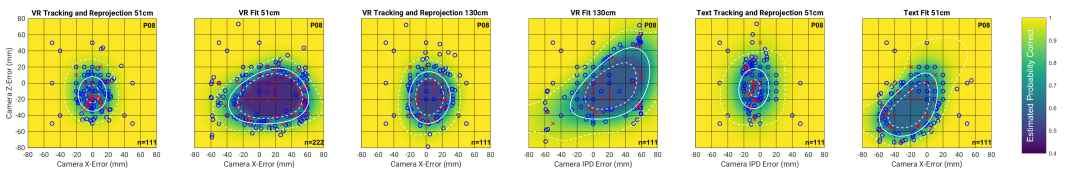


Fig. 21. P08 Raw data for near and far display distances for VR conditions.

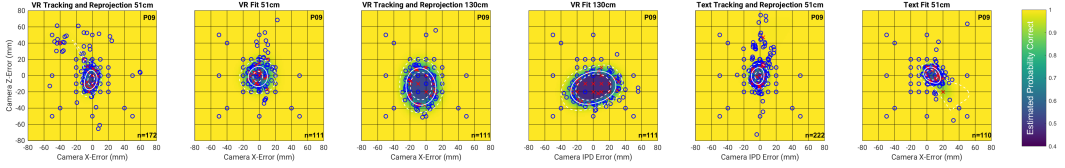


Fig. 22. P09 Raw data for near and far display distances for VR conditions.

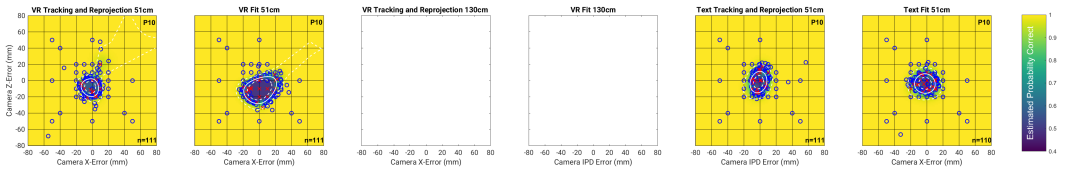


Fig. 23. P10 Raw data for near and far display distances for VR conditions.

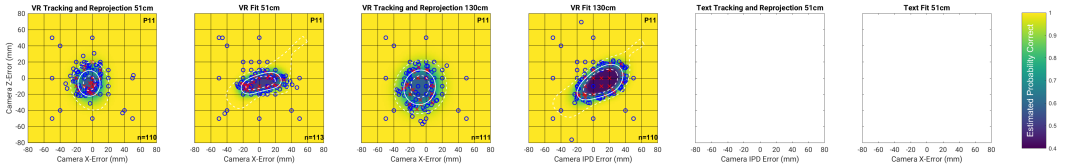


Fig. 24. P11 Raw data for near and far display distances for VR conditions.

## 2 USER STUDY TESTBED

### 2.1 Bite Bar Calibration Hardware

This CAD design shows the entire platform. Note that four beamsplitters (transparent cubes) shown allow us to replicate the sighting protocol from Hillis and Banks [2001], but were not used in our final bite bar fabrication procedure.

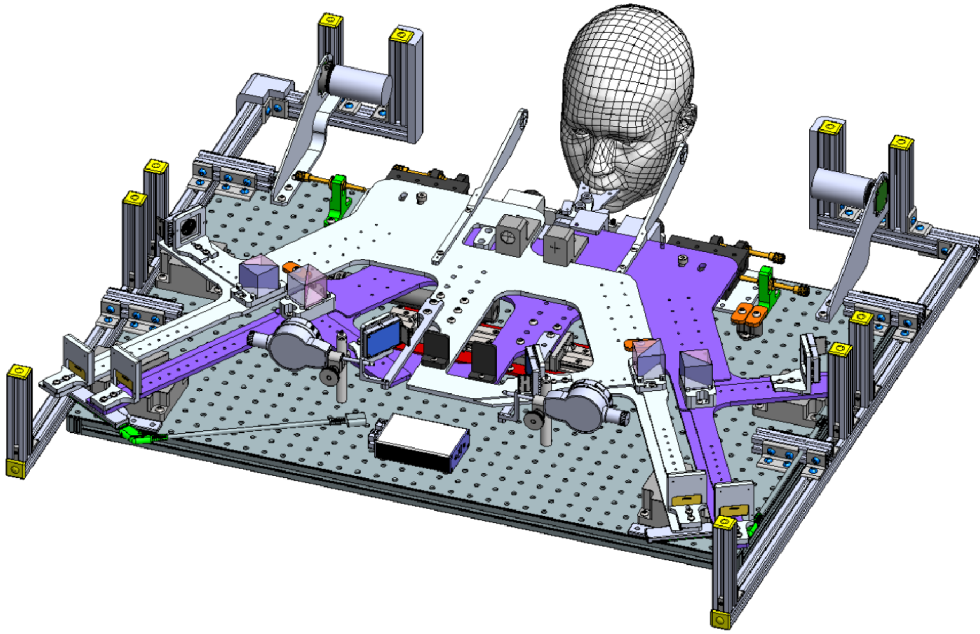


Fig. 25. CAD of Bite bar calibration platform.

## REFERENCES

- Jacob R. Gardner, Xinyu D. Song, Kilian Q. Weinberger, Dennis Barbour, and John P. Cunningham. 2015. Psychophysical detection testing with Bayesian active learning. *Uncertainty in Artificial Intelligence - Proceedings of the 31st Conference, UAI 2015* (2015), 286–295.
- Phillip Guan, Olivier Mercier, Michael Shvartsman, and Douglas Lanman. 2022. Perceptual Requirements for Eye-Trackled Distortion Correction in VR. In *ACM SIGGRAPH 2022 Conference Proceedings* (Vancouver, BC, Canada) (SIGGRAPH '22). Association for Computing Machinery, New York, NY, USA, Article 51, 8 pages. <https://doi.org/10.1145/3528233.3530699>
- James M. Hillis and Martin S. Banks. 2001. Are corresponding points fixed? *Vision Research* 41, 19 (2001), 2457–2473. [https://doi.org/10.1016/S0042-6989\(01\)00137-7](https://doi.org/10.1016/S0042-6989(01)00137-7)
- Lizhen Lin and David B. Dunson. 2014. Bayesian monotone regression using Gaussian process projection. *Biometrika* 101, 2 (2014), 303–317. <https://doi.org/10.1093/biomet/ast063>
- Lucy Owen, Jonathan Browder, Benjamin Letham, Gideon Stocek, Chase Tymms, and Michael Shvartsman. 2021. Adaptive Nonparametric Psychophysics. arXiv:2104.09549 [stat.ME]